An Adaptive Cascade Control Design for a Tracked Solar Panel Cleaning Robot

Yuliyanto Agung Prabowo
Department of Electrical Engineering, Institut Teknologi Adhi Tama Surabaya, Surabaya, Indonesia
agungp@itats.ac.id (corresponding author)

Riza Agung Firmasnyah
Department of Electrical Engineering, Institut Teknologi Adhi Tama Surabaya, Surabaya, Indonesia
rizaagungf@itast.ac.id

Ilmiatul Masfufiah
Department of Electrical Engineering, Institut Teknologi Adhi Tama Surabaya, Surabaya, Indonesia
i.masfufiah@itast.ac.id

Ilmi Rizki Imaduddin
Department of Electrical Engineering, Universitas Nurul Jadid, Probolinggo, Indonesia
ilmi.eeunuja@gmail.com

Received: 25 September 2025 | Revised: 12 January 2026 and 29 January 2026 | Accepted: 31 January 2026

 DOI: https://doi.org/10.48084/etasr.15107

ABSTRACT

The degradation of solar panel efficiency due to the accumulation of dust and contaminants presents a serious challenge in optimizing renewable energy systems. To address this issue, the current study proposes the design of a cascade control strategy employing a Proportional-Integral (PI) controller in the inner loop and an adaptive backstepping controller in the outer loop for a tracked-type solar panel cleaning robot. Dynamic and kinematic models were derived based on a tracked robot modeling approach. Trajectory tracking tests were conducted using a curved trajectory. The results demonstrate that the proposed control system achieved a tracking error of 0.017 m along the curved path. The control signals exhibited stable and responsive actuation performance. This strategy is effective in enhancing motion accuracy and stability of the robot in solar panel cleaning scenarios involving various trajectory shapes. Furthermore, this research highlights the potential of adaptive control implementation for field robotic systems that require robustness against dynamic uncertainties and terrain variations.

Keywords-solar panel; tracked robot; nonlinear system; cascade control; adaptive backstepping

I. INTRODUCTION

The utilization of solar energy as a renewable energy source addresses the challenges of the energy crisis and climate change. Solar panels or photovoltaic modules are the core components of solar power systems, converting sunlight into electrical energy. One of the most common technical issues in these systems is the reduction in efficiency due to the accumulation of dust, pollutants, and other debris on the panel surface. Dirt accumulation can reduce panel efficiency by more than 30%, depending on the location and weather conditions [1]. On a large scale, manual cleaning of solar panels is not only inefficient but also incurs high operational costs and significant safety risks. Consequently, various automation-based approaches have been developed, including the use of mobile robots equipped with automatic cleaning systems. Among the available designs, tracked robots constitute a suitable choice for this application due to their mobility on inclined surfaces, stability on slippery areas, and even weight distribution [2]. However, the motion control of tracked robots has its own challenges, particularly due to the nonlinear nature of the system, the presence of longitudinal slip, and model uncertainties arising from terrain variations. Cascade control approaches have been widely adopted to address these issues. The cascade structure enables the separation of system control into two hierarchical levels: an outer loop for regulating kinematics (position and orientation) and an inner loop for controlling dynamics (velocity and torque). This approach has been shown to improve the tracking performance and facilitate the integration of linear and nonlinear control strategies [3].

Cascade control architectures have been implemented in robotic systems and electric drives using layered controller configurations. It has been demonstrated that a cascade

structure with the outer loop acting as a position controller and the inner loop as a velocity controller provides greater stability against system parameter variations [4]. Another approach applied a combination of Sliding Mode Control (SMC) in the outer loop and Model Predictive Control (MPC) in the inner loop to achieve high-precision trajectory tracking, although controller complexity remained a significant challenge [5]. Even though these approaches yielded satisfactory performance, they were not fully adaptive to changing terrain conditions or dynamic uncertainties.

Backstepping control is a well-established nonlinear control technique, which is employed in mobile robot control and systems with complex dynamics. This method offers a systematic, Lyapunov-based, and recursive design framework, making it suitable for systems with sequential dynamics, such as wheeled and tracked robots [3]. In practice, backstepping control has been successfully applied to regulate robot velocity and position in controlled environments, including linear path-following and direction-based maneuvering scenarios [6]. Moreover, this control design has demonstrated the ability to suppress minor disturbances and maintain tracking stability when the system model is well known [4]. However, its effectiveness strongly depends on model accuracy and fixed system parameters. In real-world applications, factors such as mass variation, dynamic friction, and changing surface conditions can lead to performance degradation in the absence of parameter adaptation mechanisms. Therefore, there is a need to develop adaptive backstepping approaches capable of adjusting control actions online in response to actual system dynamics. Adaptive backstepping control has been proven effective in handling nonlinear systems affected by complex dynamics and time-varying parameters. Adaptive backstepping controllers have been integrated with Extended State Observers (ESO), enabling real-time estimation of external disturbances and maintaining stable robot position and orientation under varying load and terrain conditions [7]. Research on underwater vehicles has shown that this method can preserve motion stability and reduce tracking errors despite model inaccuracies and unknown disturbances [8]. Similarly, in wheeled robot applications, this technique enables real-time adaptation of velocity and steering parameters during operation [9]. Furthermore, integration with SMC has been shown to enhance the efficiency against measurement noise and environmental disturbances [10]. Overall, adaptive backstepping offers significant advantages in achieving accurate, responsive, and effective control performance under uncertain conditions, rendering it a highly relevant solution for tracked-type solar panel cleaning robots.

This study introduces a novel contribution by applying adaptive backstepping control to the outer loop of a tracked solar panel cleaning robot control system. The proposed approach is designed to address nonlinear dynamics, parameter uncertainties, and frequent terrain variations encountered in outdoor applications. Unlike previous studies that employed linear control or conventional backstepping methods, this approach integrates adaptive mechanisms that enable real-time parameter adjustments. As a result, the system can maintain accurate position tracking, stable orientation control, and efficient actuator signal utilization, positioning this strategy as a significant contribution to the advancement of mobile robot control systems.

II. SYSTEM MODELING

Two reference frames were employed in the analysis, namely the global frame G and the local body-fixed frame B, as illustrated in Figure 1. The global frame G is defined as fixed with respect to the ground surface, with its origin located at the robot's center of gravity at the initial condition. In contrast, the local frame B is attached to the robot's center of gravity and moves along with the robot, following its orientation and motion.

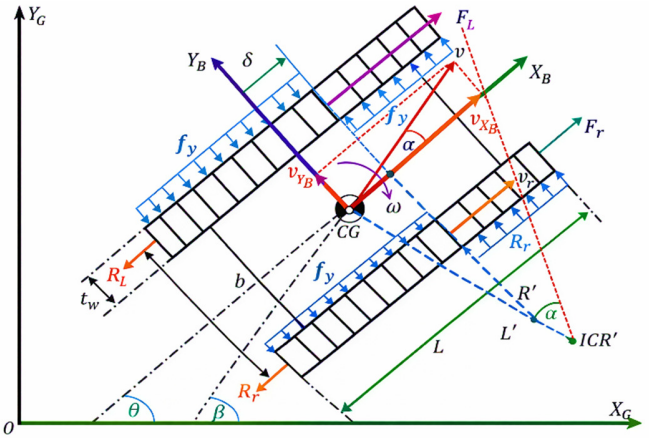

Fig. 1. Reference frames in kinematic and dynamic modeling.

A. Tracked Robot Kinematic Model

The kinematic model of a tracked robot describes the relationship between the linear and angular velocities and the robot's position and orientation in a two-dimensional plane. This model accounts for the track slip effect, which causes a displacement of the Instantaneous Center of Rotation (ICR) by a distance of δ [4]. The actual linear velocities of the left and right tracks are expressed as:

$$v_L = r\omega_L(1-\sigma_L), v_R = r\omega_R(1-\sigma_R) \quad (1)$$

where σ_L and σ_R represent the slip ratios of the left and right tracks, respectively, which depend on the angular velocity and traction radius. In the global reference frame G, the robot velocity can be expressed by considering longitudinal slip (σ_L, σ_R) and the lateral slip angle (α). The translational and rotational velocity models are given by:

$$\begin{bmatrix}\dot{x}\\ \dot{y}\\ \dot{\theta}\end{bmatrix} = \frac{r}{2}T(\theta,\alpha)\begin{bmatrix}\omega_L(1-\sigma_L)\\ \omega_R(1-\sigma_R)\end{bmatrix} \quad (2)$$

where:

$$T(\theta,\alpha) = \begin{bmatrix}\cos\theta - \sin\theta\tan\alpha & \sin\theta + \cos\theta\tan\alpha\\ \sin\theta + \cos\theta\tan\alpha & -\cos\theta + \sin\theta\tan\alpha\\ -\frac{2}{b} & \frac{2}{b}\end{bmatrix} \quad (3)$$

Since the vehicle can only move in the direction normal to the sprocket axis, a nonholonomic constraint applies and is formulated as [4]:

$$-\dot{x}\sin\theta + \dot{y}\cos\theta + \delta\dot{\theta} = 0 \quad (4)$$

In order to express the model in a homogeneous form, generalized coordinates are utilized:

$$q(t) = \begin{bmatrix} x \\ y \\ R_g\theta \end{bmatrix} \quad (5)$$

The nonholonomic constraint expressed in (4) can be reformulated in matrix form as:

$$A^T(q)\dot{q} = 0, A(q) = \begin{bmatrix} -\sin\theta \\ \cos\theta \\ \delta/R_g \end{bmatrix} \quad (6)$$

To ensure that the system is controllable, a matrix $S(q)$ that is orthogonal to $A(q)$ is developed:

$$S^T(q)A(q) = 0 \quad (7)$$

Accordingly, the vector of position and orientation rate $\dot{q}$ can be expressed as a function of the velocity vector $V(t) = [v, \dot{\theta}]^T$:

$$\dot{q} = S(q)V(t) \quad (8)$$

The explicit form of the matrix $S(q)$ is given as:

$$S(q) = \begin{bmatrix} \cos\theta & (\delta/R_g)\sin\theta \\ \sin\theta & -(\delta/R_g)\cos\theta \\ 0 & 1 \end{bmatrix} \quad (9)$$

B. Tracked Robot Dynamic Model

The dynamic model of the tracked robot was developed to represent the interaction between the mechanical forces and translational and rotational motion dynamics of the vehicle. In the robot body frame, the longitudinal and lateral accelerations are generated by the traction forces of the left and right tracks (F_L, F_R), as well as the longitudinal resistance forces acting on the left and right tracks (R_L, R_R). In addition, the lateral friction force (F_y) contributes to the lateral acceleration. It is assumed that the normal pressure distribution is uniform and that the lateral resistance coefficient μ_t remains constant [4]. The rotational dynamics about the yaw axis are governed by the total driving moment M and the resistive moment M_r. The fundamental equations of motion in the body frame are expressed as:

$$m\ddot{y}_{\mathbb{B}} = F_y \quad (10)$$

$$I_z\ddot{\theta} = M - M_r \quad (11)$$

The traction force of each track was derived from the motor torque constant and wheel radius:

$$F_L = \frac{\tau_L}{r}, F_R = \frac{\tau_R}{r} \quad (12)$$

The longitudinal resistance force is determined by the normal load on the track and the surface static friction coefficient μ_l:

$$R_L = \mu_l\left(\frac{W}{2}\right), R_R = \mu_l\left(\frac{W}{2}\right) \quad (13)$$

The lateral friction force F_y is derived from the normal force distribution, the lateral friction coefficient μ_t, and the track contact length L, and is expressed as:

$$F_y = 2 \cdot \mathrm{sgn}(\omega) \cdot \mu_t \cdot \frac{W}{L}\left(\delta^2 - \frac{L^2}{4}\right) \quad (14)$$

The traction moment induced by the motor torque about the yaw axis is expressed as:

$$M = \frac{b}{2}(F_L + F_R) \quad (15)$$

For a systematic formulation of the dynamic model, the Euler–Lagrange method considering nonholonomic constraints is adopted [4, 6]. The general model is given by:

$$M(q)\ddot{q} + f(\dot{q}) + A(q)^T\lambda = B(q)\tau + \tau_d \quad (16)$$

where $q = [x, y, R_g\theta]^T$ represents the generalized coordinates, $M(q)$ is the inertia matrix, $f(\dot{q})$ denotes the vector of friction and resistance forces, $A(q)^T\lambda$ represents the nonholonomic constraints (Lagrange multipliers), τ is the vector of motor input torques, and τ_d denotes external disturbances.

The matrix and vector structures of the above model are derived by projecting onto the constraint-free subspace using the orthogonal matrix $S(q)$. Following constraint elimination, the dynamic system is expressed as [4, 6]:

$$\bar{M}(q)\dot{V}(t) + \bar{C}(\dot{q}, q)V(t) + \bar{f}(q) = \bar{B}(q)\tau + \tau_d \quad (17)$$

where:

$$\bar{M}(q) = \begin{bmatrix} m & 0 \\ 0 & \frac{m\delta^2 + I_z}{R_g^2} \end{bmatrix} \quad (18)$$

$$\bar{C}(\dot{q}, q) = \begin{bmatrix} 0 & -\frac{m\delta\dot{\theta}}{R_g} \\ 0 & \frac{m\delta\dot{\theta}}{R_g^2} \end{bmatrix} \quad (19)$$

$$\bar{f}(q) = \begin{bmatrix} \frac{R_L + R_R}{2} \\ \frac{F_y\delta + M_r}{R_g} \end{bmatrix} \quad (20)$$

$$\bar{B}(q) = \begin{bmatrix} 1 & 1 \\ \frac{b}{2R_g} & -\frac{b}{2R_g} \end{bmatrix} \quad (21)$$

III. CONTROL DESIGN

The cascade control strategy for a tracked-type solar panel cleaning robot represents a hierarchical approach that divides the control structure into two levels to enhance the system performance in the presence of nonlinear dynamics and environmental uncertainties. The outer loop employs a PI controller to generate linear velocity (v) and angular velocity (ω) references based on the position error relative to the target, while the inner loop utilizes an adaptive backstepping method to efficiently regulate the velocity dynamics and actuator torques. This approach enables improved tracking accuracy, steady-state error attenuation, and robustness against terrain variations. The combination of PI and backstepping controllers

within a cascade structure has been demonstrated to significantly enhance the stability of nonlinear robotic systems. This control architecture is particularly well suited for applications on inclined and slippery solar panel surfaces. Figure 2 illustrates the block diagram of the proposed control system.

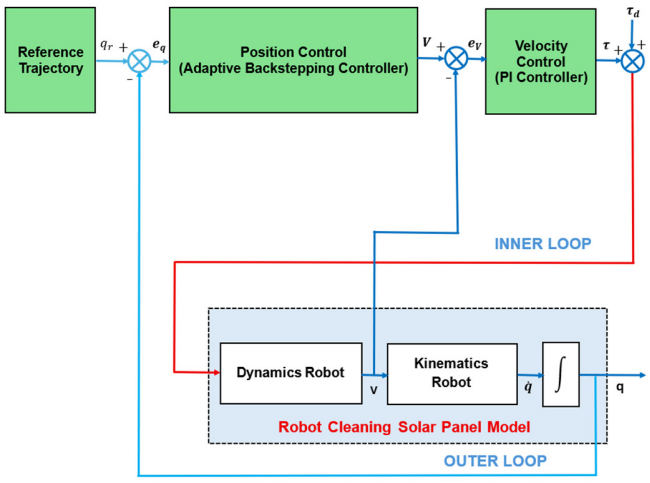

Fig. 2. Cascade control block diagram for a solar panel cleaning robot.

A. *Inner-Loop Design: PI-Based Dynamic Control*

In the cascade control system of a tracked-type solar panel cleaning robot, the inner loop is responsible for regulating the robot's motion dynamics, namely the linear velocity v and the angular velocity ω. This control action is performed based on the velocity references v_{ref} and ω_{ref} generated by the outer loop, by comparing them with the actual velocities measured from the system. The difference between the reference and actual values is defined as the velocity error signal:

$$e_v = v_{\text{ref}} - v, e_\omega = \omega_{\text{ref}} - \omega \quad (22)$$

To minimize this error effectively, a PI controller was adopted owing to its ability to eliminate steady-state errors and enhance system stability. The PI control law for generating the actuator torque signals τ_L and τ_R is expressed as:

$$\tau_L = K_{pv}e_v + K_{iv}\int e_v\, dt - \left(K_{p\omega}e_\omega + K_{i\omega}\int e_\omega\, dt\right) \quad (23)$$

$$\tau_R = K_{pv}e_v + K_{iv}\int e_v\, dt + \left(K_{p\omega}e_\omega + K_{i\omega}\int e_\omega\, dt\right) \quad (24)$$

where K_{pv} and K_{iv} are the PI gains for the linear velocity control, and $K_{p\omega}$ and $K_{i\omega}$ are the PI gains for the angular velocity control. This approach is designed to generate torque signals that are applied as inputs to the robot dynamic model, which subsequently determines the acceleration and the evolution of the system's actual velocities. The left and right torque structures are symmetrically designed with differential components related to the angular velocity, thereby facilitating turning maneuvers and directional control.

B. *Outer-Loop Design: Kinematic Control Based on Adaptive Backstepping*

The position control of the solar panel cleaning robot was implemented in the outer loop using a kinematic adaptive backstepping controller. The primary objective of this controller is to ensure accurate tracking of the reference position trajectory x_d, y_d, θ_d despite the presence of kinematic parameter uncertainties and environmental disturbances, such as track slip and variations in the contact conditions of the solar panel surface.

The nonholonomic kinematic model of the tracked robot can be written as:

$$\begin{aligned} \dot{x} &= v\cos\,\theta \\ \dot{y} &= v\sin\,\theta \\ \dot{\theta} &= \omega \end{aligned} \quad (25)$$

where v and ω denote the linear and angular velocities of the robot, respectively. For controller design purposes, the position error is defined in the robot body frame as:

$$\begin{bmatrix} e_x \\ e_y \\ e_\theta \end{bmatrix} = \begin{bmatrix} \cos\theta & \sin\theta & 0 \\ -\sin\theta & \cos\theta & 0 \\ 0 & 0 & 1 \end{bmatrix} \begin{bmatrix} x_d - x \\ y_d - y \\ \theta_d - \theta \end{bmatrix} \quad (26)$$

where e_x, e_y and e_θ represent the longitudinal, lateral, and orientation errors, respectively. To guarantee system stability, a Lyapunov candidate function is selected as [7, 11]:

$$V = \frac{1}{2}e_x^2 + \frac{1}{2}e_y^2 + \frac{1}{2}e_\theta^2 \quad (27)$$

The time derivative of the Lyapunov function is derived as:

$$\dot{V} = e_x\dot{e}_x + e_y\dot{e}_y + e_\theta\dot{e}_\theta \quad (28)$$

In the adaptive backstepping approach, the linear and angular reference velocities are designed by incorporating the adaptive parameter estimates $\hat{k}_1$, $\hat{k}_2$, and $\hat{k}_3$ as:

$$v_{ref} = v_d\cos\,e_\theta + \hat{k}_1 e_x \quad (29)$$

$$\omega_{ref} = \omega_d + \hat{k}_2 e_y + \hat{k}_3\sin\,e_\theta \quad (30)$$

where v_d and ω_d denote the velocity references generated by the trajectory planner. The parameters $\hat{k}_i$represent online estimates of the control parameters, which are updated using adaptation laws, as described in [9, 10].

In order to guarantee that $\dot{V} \leq 0$, the adaptation laws are defined as:

$$\dot{\hat{k}}_1 = \gamma_1 e_x^2 \quad (31)$$

$$\dot{\hat{k}}_2 = \gamma_2 e_y^2 \quad (32)$$

$$\dot{\hat{k}}_3 = \gamma_3\sin^2 e_\theta \quad (33)$$

where $\gamma_1, \gamma_2, \gamma_3 > 0$ are the adaptation gains. By substituting the control laws and the adaptation laws into the time derivative of the Lyapunov function, it is shown that $\dot{V}$ is negative semidefinite, thereby guaranteeing Lyapunov stability of the system and convergence of the position errors to zero.

IV. RESULTS

The robot parameters used in the experiments are listed in Table I.

TABLE I. PARAMETERS OF THE SOLAR PANEL CLEANING ROBOT

Parameter	Symbol	Value	Unit
Length	p	0.27	m
Width	l	0.255	m
Height	t	0.09	m
Sprocket radius	r	0.0156	m
Distance between wheels	L	0.15	m
Robot mass	m	5.0	kg
Yaw inertia moment	I_z	0.2	kg·m²
Viscous friction	B	0.05	Nms/rad
Longitudinal friction	μ_s	0.05	–
Transversal friction	μ_t	0.03	–

To evaluate the performance of the proposed cascade control strategy on the solar panel cleaning robot system, experiments were conducted using motion trajectories that represent realistic cleaning scenarios. The tested trajectory follows a curved path resembling a circular cleaning pattern. This experiment aimed to assess the controller's capability in maintaining positional accuracy and dynamic stability during continuous maneuvering conditions. All physical and control parameters obtained from the preliminary tests were consistently applied to ensure coherence between the developed model and its actual implementation.

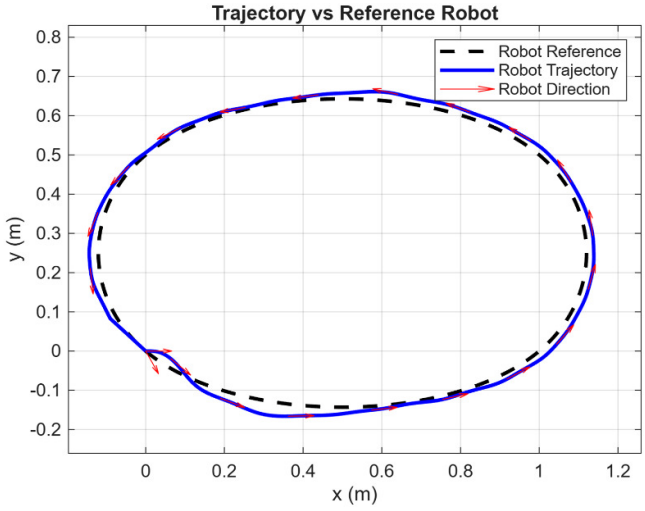

Fig. 3. Results of trajectory tracking experiments.

In the curved-trajectory experiment, the robot was commanded to follow an elliptical path to represent comprehensive solar panel cleaning coverage, as illustrated in Figures 3 and 4, which show the XY-axis position response. The results indicate that the implemented cascade control system is able to maintain stable and accurate trajectory tracking despite variations in orientation and velocity throughout the motion. The recorded position tracking error of 0.017 m remained within the acceptable tolerance limits for precision cleaning applications, demonstrating the effectiveness of the proposed control strategy in handling nonlinear motion and dynamic trajectory changes.

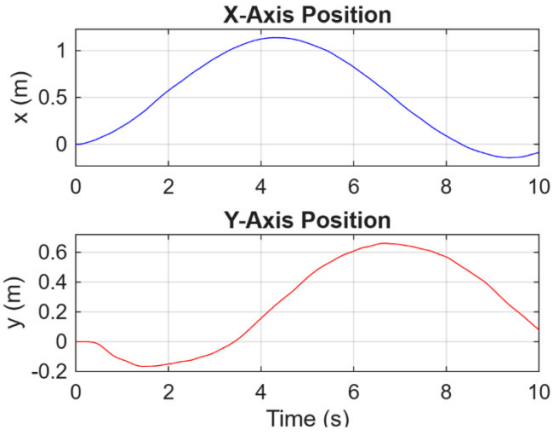

Fig. 4. XY-axis position response.

The linear and angular velocity responses exhibited adaptive behavior in response to changes in orientation, with velocity fluctuations remaining well regulated, as displayed in Figure 5. These results confirm that the integration of PI control in the inner loop and adaptive backstepping in the outer loop effectively handles complex and nonlinear maneuvering conditions, while maintaining actuation efficiency and overall system stability. Furthermore, the smooth velocity profiles indicate that the control strategy successfully limits abrupt actuator commands, thereby reducing the risk of excessive mechanical stress and improving operational safety during continuous cleaning tasks.

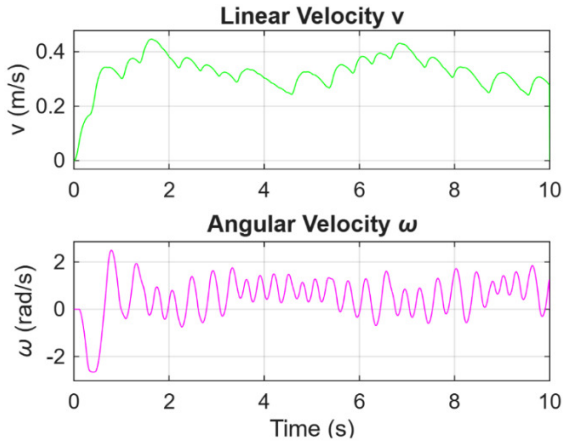

Fig. 5. Linear and angular velocity response.

V. CONCLUSIONS

Based on the experimental results, the cascade control strategy employing a Proportional-Integral (PI) controller in the inner loop and an adaptive backstepping controller in the outer loop demonstrated excellent performance in controlling the tracked-type solar-panel cleaning robot. Along the curved trajectory, the tracking error was well-controlled at 0.017 m. The linear and angular velocity responses exhibited stable and adaptive behaviors in response to reference changes, indicating that the control system operated efficiently and safely under dynamic loading conditions.

ACKNOWLEDGMENTS

The authors would like to express their gratitude to the Ministry of Higher Education, Science, and Technology of the Republic of Indonesia for its support through funding from the 2025 Regular Fundamental Research Program under Contract Number 128 / C3 / DT.05.00 / PL / 2025; 095 / LL7 / DT.05.00 /PL/2025 and 05/05.LITI/LPPM/ITATS/PL/2025. This support enabled the successful implementation of this research in accordance with the planned objectives.

REFERENCES

[1] M. Mani and R. Pillai, "Impact of dust on solar photovoltaic (PV) performance: Research status, challenges and recommendations," *Renewable and Sustainable Energy Reviews*, vol. 14, no. 9, pp. 3124–3131, Dec. 2010, https://doi.org/10.1016/j.rser.2010.07.065.

[2] J. Gao, Y. Li, J. Jin, Z. Jia, and C. Wei, "Design, Analysis and Control of Tracked Mobile Robot with Passive Suspension on Rugged Terrain," *Actuators*, vol. 14, no. 8, Aug. 2025, Art. no. 389, https://doi.org/10.3390/act14080389.

[3] H. Zhang and N. M. Nor, "Control Strategies for Two-Wheeled Self-Balancing Robotic Systems: A Comprehensive Review," *Robotics*, vol. 14, no. 8, July 2025, Art. no. 101, https://doi.org/10.3390/robotics14080101.

[4] A. D. Sabiha, M. A. Kamel, E. Said, and W. M. Hussein, "ROS-based trajectory tracking control for autonomous tracked vehicle using optimized backstepping and sliding mode control," *Robotics and Autonomous Systems*, vol. 152, June 2022, Art. no. 104058, https://doi.org/10.1016/j.robot.2022.104058.

[5] Y. Du *et al.*, "High-Precision Trajectory Tracking System for Fork-Shaped Mobile Robot Based on Cascade S_MPC Control," in *2024 IEEE 14th International Conference on CYBER Technology in Automation, Control, and Intelligent Systems*, Copenhagen, Denmark, July 2024, pp. 752–756, https://doi.org/10.1109/CYBER63482.2024.10748748.

[6] A. Ahmed, M. A. Kamel, E. Said, and A. Roshdy, "Modeling and Optimal Trajectory Tracking Control of an Autonomous Tracked Mobile Robot Using a Modified PID Controller and Backstepping," *Journal of Physics: Conference Series*, vol. 3058, July 2025, Art. no. 012005, https://doi.org/10.1088/1742-6596/3058/1/012005.

[7] K. Wang, Y. Liu, C. Huang, and P. Cheng, "Adaptive Backstepping Control with Extended State Observer for Wheeled Mobile Robot," in *2020 39th Chinese Control Conference*, Shenyang, China, July 2020, pp. 1981–1986, https://doi.org/10.23919/CCC50068.2020.9188593.

[8] W. C. Yang, P. Z. Du, R. Y. Hu, Y. Q. Wang, D. W. Xu, and S. H. Huang, "Adaptive Backstepping Sliding Mode Attitude Control for AUVs Subject to Model Errors and Unknown Disturbances," in *OCEANS 2022, Hampton Roads*, Hampton Roads, VA, USA, Oct. 2022, pp. 1–5, https://doi.org/10.1109/OCEANS47191.2022.9977256.

[9] S. T. Dang, X. M. Dinh, T. D. Kim, H. L. Xuan, and M.-H. Ha, "Adaptive Backstepping Hierarchical Sliding Mode Control for 3-Wheeled Mobile Robots Based on RBF Neural Networks," *Electronics*, vol. 12, no. 11, May 2023, Art. no. 2345, https://doi.org/10.3390/electronics12112345.

[10] Z. Jinlong *et al.*, "Control Design of the Quadrotor Aircraft based on the Integral Adaptive Improved Integral Backstepping Sliding Mode Scheme," *Engineering, Technology & Applied Science Research*, vol. 14, no. 5, pp. 17106–17117, Oct. 2024, https://doi.org/10.48084/etasr.8361.

[11] S. Rudra, K. Ghosh, and M. Das, "Robust adaptive integral backstepping control and its implementation on motion control system," in *2012 International Conference on Power, Signals, Controls and Computation*, Thrissur, Kerala, India, Jan. 2012, pp. 1–6, https://doi.org/10.1109/EPSCICON.2012.6175279.